Science Advances

AAAS

advances.sciencemag.org/cgi/content/full/3/6/e1603206/DC1

Supplementary Materials for

Two orders of magnitude enhancement in oxygen evolution reactivity on amorphous $Ba_{0.5}Sr_{0.5}Co_{0.8}Fe_{0.2}O_{3-\delta}$ nanofilms with tunable oxidation state

Gao Chen, Wei Zhou, Daqin Guan, Jaka Sunarso, Yanping Zhu, Xuefeng Hu, Wei Zhang, Zongping Shao

Published 21 June 2017, *Sci. Adv.* **3**, e1603206 (2017)
DOI: 10.1126/sciadv.1603206

The PDF file includes:

- table S3. Comparison of the performance of the water-splitting catalysts in a 1.0 M KOH solution.
- Legend for movie S1
- References (*33*–*47*)

Other Supplementary Material for this manuscript includes the following:
(available at advances.sciencemag.org/cgi/content/full/3/6/e1603206/DC1)

- movie S1 (.mp4 format). Video of a water-splitting device.

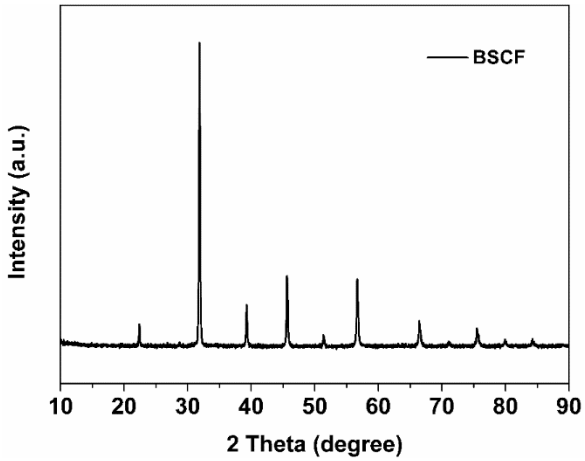

fig. S1. Powder XRD patterns of the crystalline BSCF perovskite target.

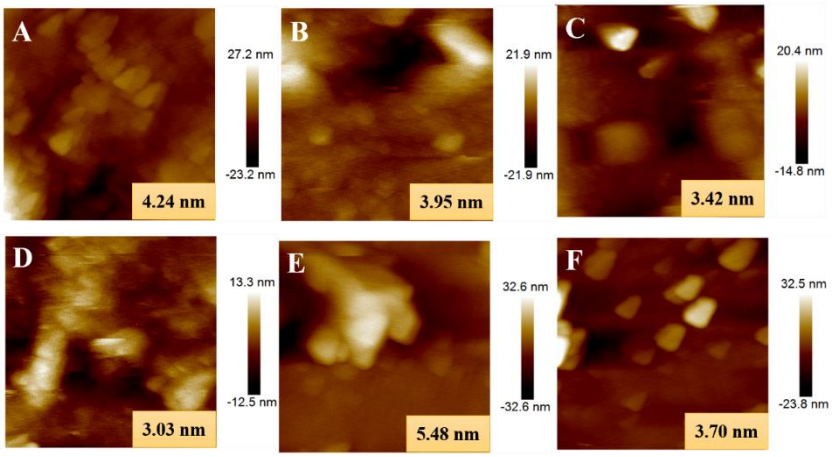

fig. S2. Surface morphology obtained by AFM on the top of Ni foil. (**A**) Substrate, (**B**) 1 nm, (**C**) 5 nm, (**D**) 10 nm, (**E**) 15 nm and (**F**) 20 nm thick BSCF nanofilm. The inset numbers correspond to the surface roughness (in nm).

The blue line indicates the AFM scan area while the yellow line represents the three-dimensional (3-D) surface of the entire AFM area. The 3-D surface area was obtained by triangulation of neighboring pixels. This value is derived from the AFM data analyzed by NanoScope Analysis. The surface calibration factor was calculated from the 3-D surface area divided by the AFM scan area. (Ref. 15)

To obtain the intrinsic activities, the surface areas of the thin films were corrected to the 3-D surface of the entire AFM area. The surface areas of Ni foil and Ni-based 1-20 nm thin films should be multiplied by 1.04, 1.05, 1.02, 1.03, 1.06, and 1.03. The ITO-based 1-15 nm thin films should be multiplied by 1.03, 1.02, 1.03, 1.01, and 1.02.

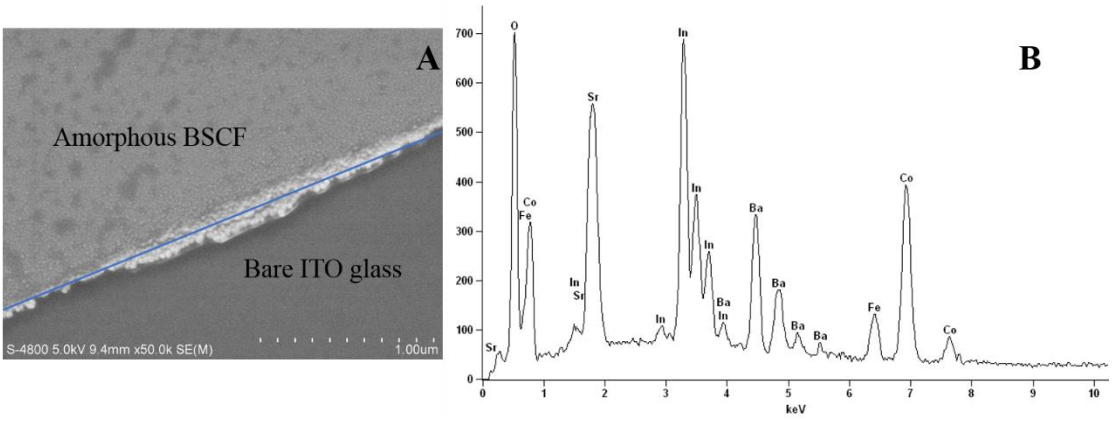

fig. S3. SEM image of the amorphous BSCF nanofilm and the respective energy-dispersive x-ray spectrum.

The energy dispersive X-ray spectrum indicates a Ba: Sr: Co: Fe ratio of 0.35: 0.5: 0.81: 0.23, which is close to the target Ba: Sr: Co: Fe stoichiometric ratio of 0.5: 0.5: 0.8: 0.2.

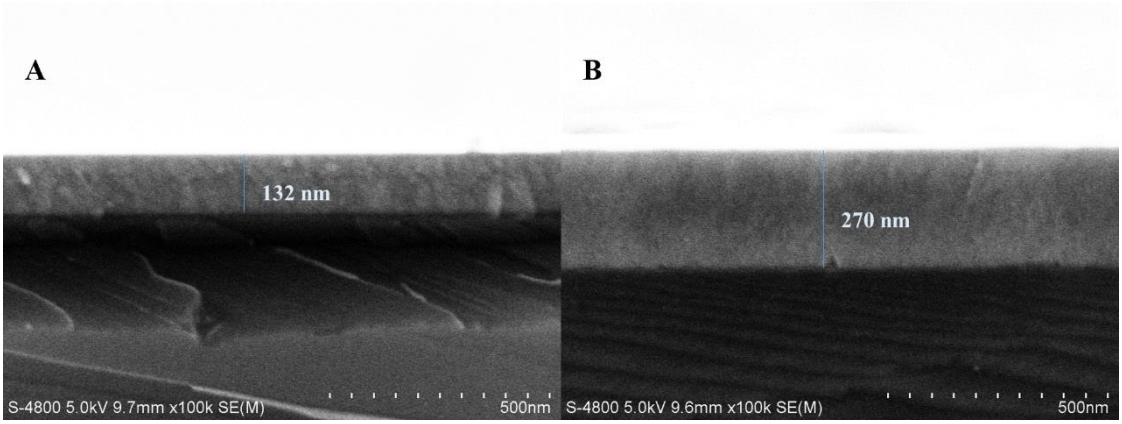

fig. S4. SEM images of the film/substrate interface on the top of silicon wafer. (**A**) 100 nm and (**B**) 200 nm amorphous BSCF thin film.

The scanning electron images indicate that the thicknesses are 132 nm and 270 nm for 100 nm and 200 nm amorphous BSCF, respectively. The real BSCF thickness should be approximately 1.34 times that of the target thickness. For simplicity, we use the target thickness to label the samples.

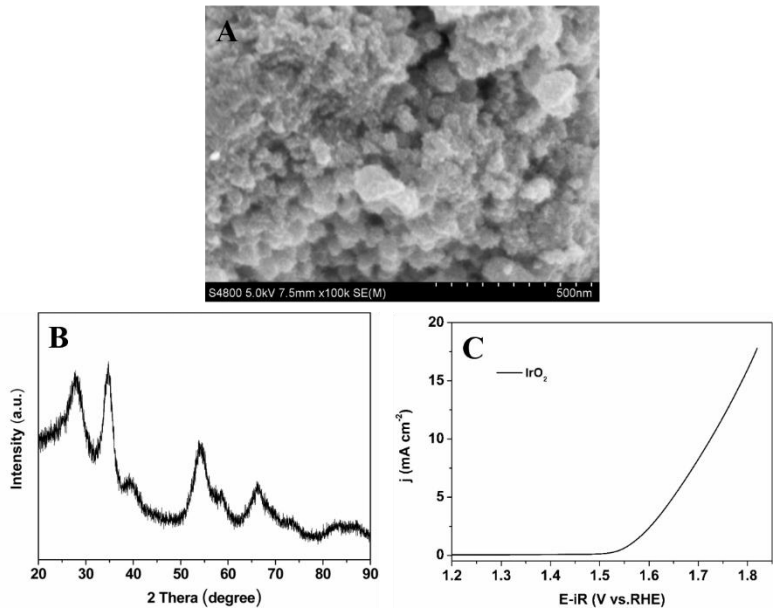

fig. S5. Basic characterizations and OER activity of bulk IrO_2. (**A**) SEM image and (**B**) Powder XRD pattern of IrO_2; (**C**) Geometric electrode area normalized OER activity for the bulk IrO_2 catalyst obtained from a traditional RDE test at 1600 rpm.

The IrO_2 (99.99% purity, surface area of 139.8 m^2 g^{-1}) catalyst was purchased from Aladdin Industrial Corporation. The particle size varies from ~60 nm to above 100 nm. The powder XRD pattern displays a tetragonal structure (space group: P42/mnm, JCPDS No. 15-0870).

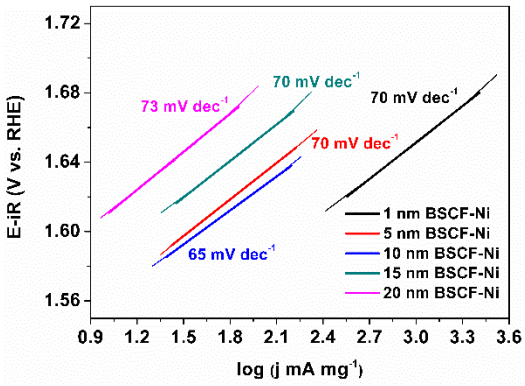

fig. S6. Tafel slopes for mass activities of amorphous BSCF on Ni foil substrates.

The Tafel slope values are consistent with the intrinsic activities' values.

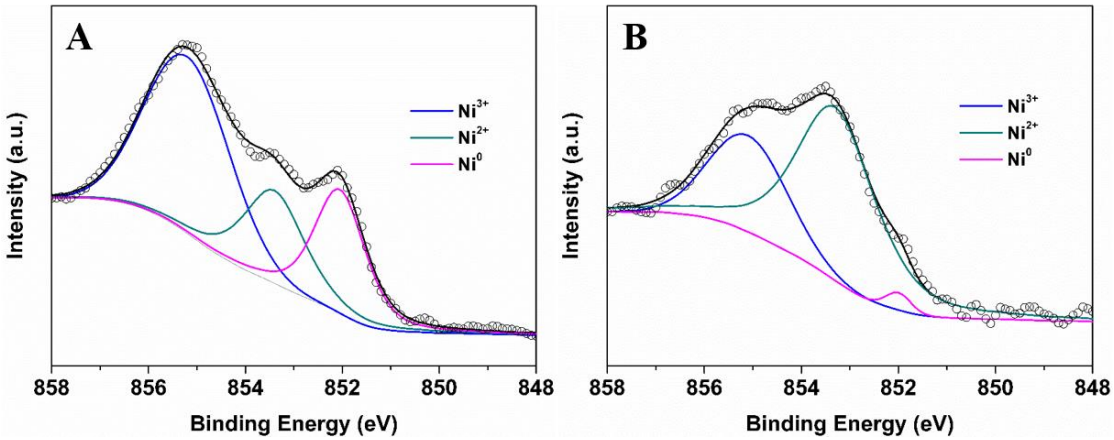

fig. S7. Ni 2p XPS. (**A**) Ni foil and (**B**) 1 nm BSCF-Ni foil heterostructure.

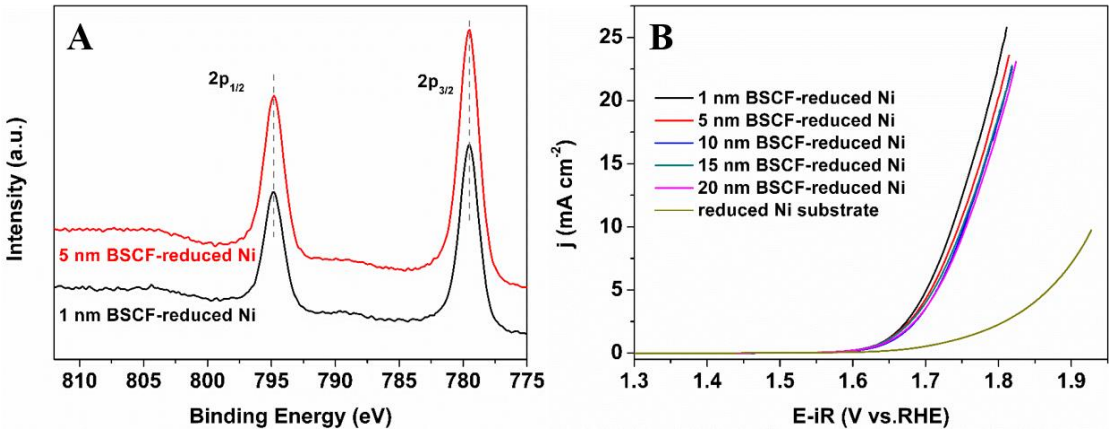

fig. S8. XPS and OER results of reduced Ni-based nanofilms. (**A**) Co 2p X-ray photoelectron spectra for the 1 nm and 5 nm thick BSCF-reduced Ni foil heterostructures. (**B**) Geometric electrode area normalized OER activities for the reduced Ni-based BSCF films.

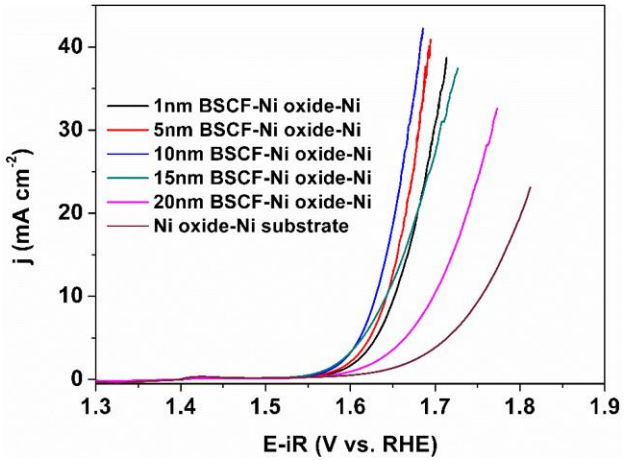

fig. S9. OER activities of Ni oxide–based nanofilms. Geometric electrode area normalized OER activities for the 1, 5, 10, 15 and 20 nm BSCF-Ni oxide-Ni foil heterostructures. The data for Ni oxide-Ni substrate are also included.

The overpotentials to achieve 10 mA cm^{-2} for the 1-20 nm BSCF-Ni oxide-Ni foil heterostructures were 0.42, 0.41, 0.4, 0.41, and 0.47 V. The 10 nm Ni oxide-Ni foil requires an overpotential of 0.52 V, which is substantially larger than those required by the BSCF thin films.

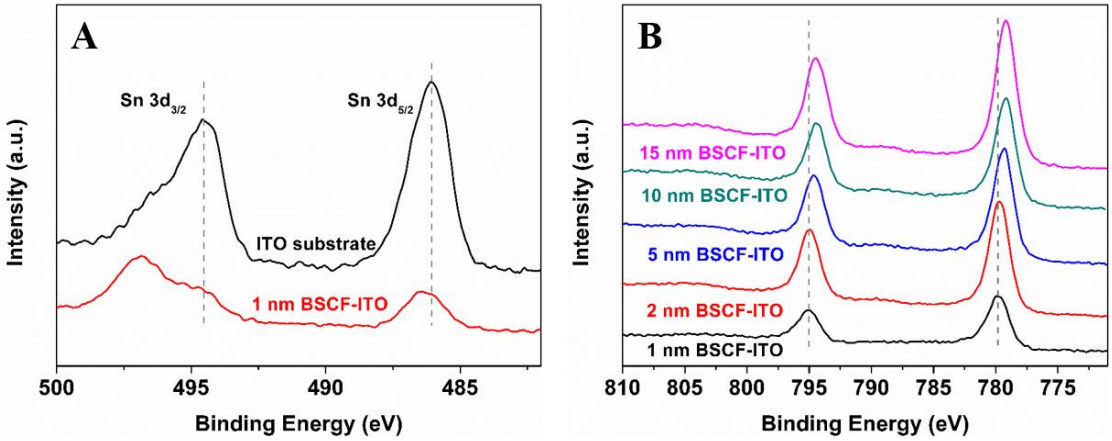

fig. S10. XPS results of ITO-based nanofilms. (**A**) Sn 3d X-ray photoelectron spectra for the 1 nm BSCF-ITO heterostructure and the ITO substrate. (**B**) Co 2p X-ray photoelectron spectra for the 1 nm, 2 nm, 5 nm, 10 nm, and 15 nm thick BSCF-ITO heterostructures.

The reduced oxidation state of the Sn ion in the ITO substrate and the shift in the Co 2p spectra of the BSCF thin films reveal the tunability of the transition metal ion in the ITO-based heterostructures.

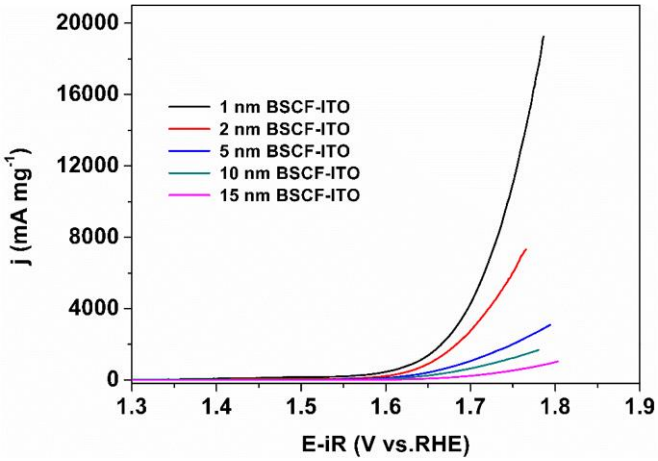

fig. S11. Mass activities for BSCF-ITO heterostructures.

The mass activities of the 1-15 nm ITO-based heterostructures at an overpotential of 0.5 V are 7810, 4548, 1618, 986 and 399 mA mg^{-1}. The mass activity of the ITO-based heterostructure is slightly lower than that of the Ni foil-based heterostructure at an identical mass loading (not including the 2 nm BSCF-ITO heterostructure).

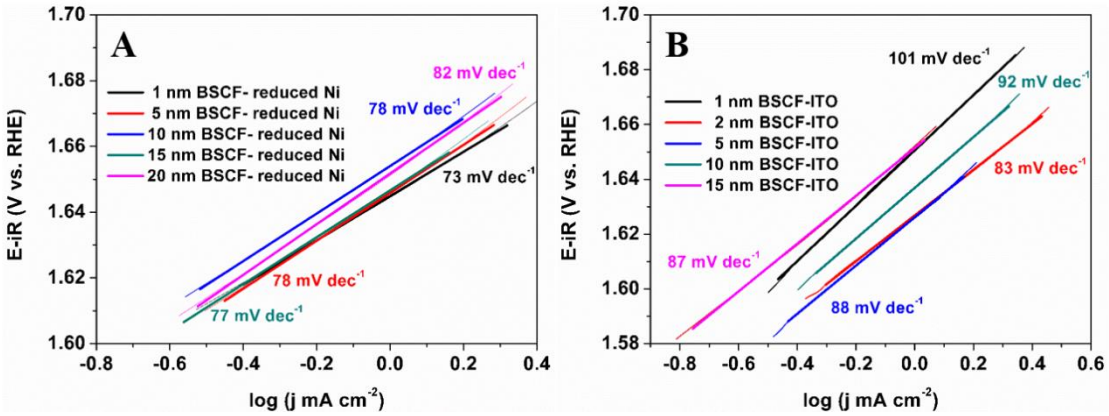

fig. S12. Tafel plots. (**A**) the 1, 5, 10, 15, and 20 nm BSCF-reduced Ni foil heterostructures and (**B**) 1, 2, 5, 10, and 15 nm BSCF-ITO glass heterostructures.

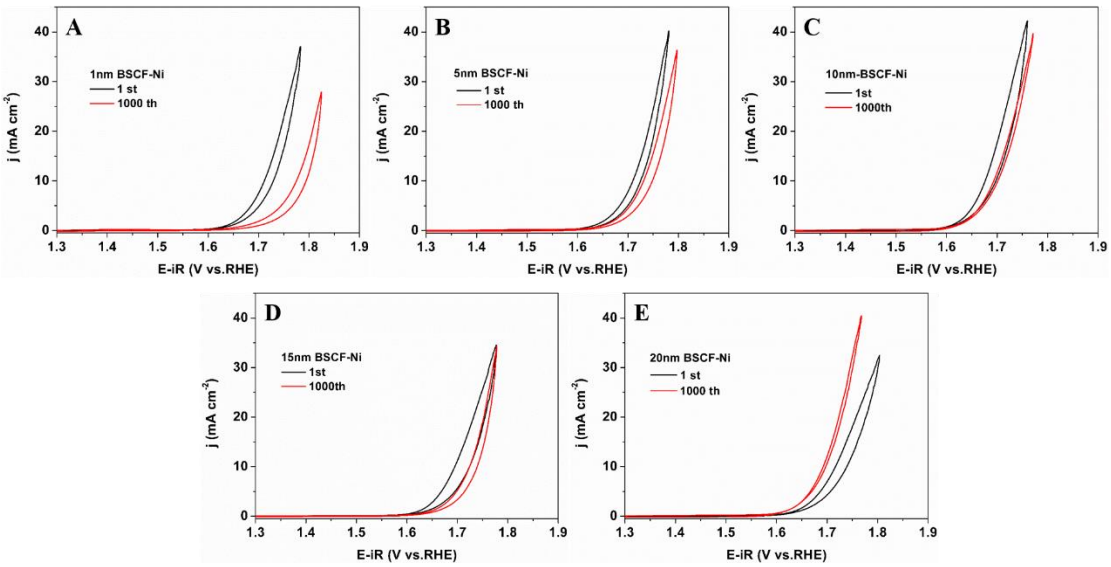

fig. S13. Stability tests of nanofilms. Current-potential profile at the 1st and 1,000th cycles for the (**A**) 1 nm, (**B**) 5 nm, (**C**) 10 nm, (**D**) 15 nm, and (**E**) 20 nm BSCF-Ni foil heterostructures electrodes.

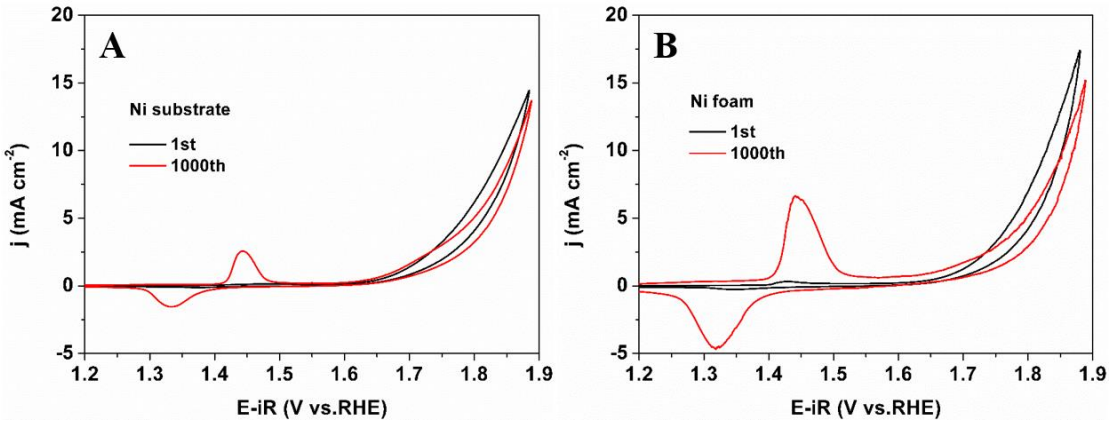

fig. S14. Stability tests of Ni foil and Ni foam. Current-potential profile at the 1st and 1,000th cycles for the (**A**) Ni foil substrate and (**B**) Ni foam substrate.

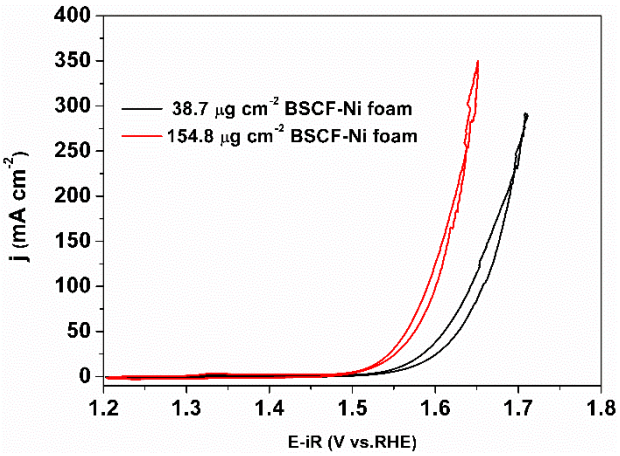

fig. S15. OER activity for the 38.7 and 154.8 μg cm^{-2} BSCF–Ni foam heterostructure electrodes in a 1.0 M KOH solution.

The onset potential of 154.8 μg cm^{-2} BSCF-Ni foam is about 1.46 V. An overpotential of ~0.29 V is required to obtain 10 mA cm^{-2}. The onset potential is 1.49 V and the overpotential to obtain 10 mA cm^{-2} is 0.34 V for 38.7 μg cm^{-2} BSCF-Ni foam.

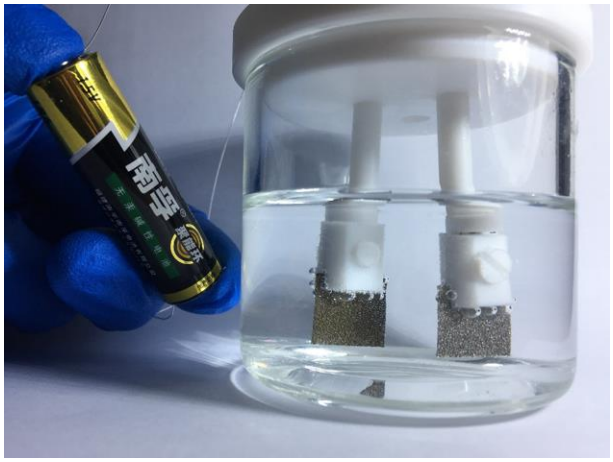

fig. S16. Photograph of a water-splitting device. Demonstration of a water-splitting device powered by an AA battery with a nominal voltage of ≈1.5 V.

table S1. Comparison of the mass activities of the thin-film heterostructures to other recently reported catalysts for the OER in an alkaline solution.

Samples	Loading ($\mu g\ cm^{-2}$)	Mass activity ($mA\ mg^{-1}$)	Overpotential (V)	Electrolyte	Reference
r-IrO_2	50	~115	~0.38	0.1 M KOH	22
SNCF	232	43	0.5	0.1 M KOH	23
BSCF	232	37	0.5	0.1 M KOH	23
SCFSn(721)	232	85	0.45	0.1 M KOH	33
LCF0.2	232	52	0.35	0.1 M KOH	30
LCO(80 nm)	250	~40	0.49	0.1 M KOH	34
Co_3O_4@CoO SC	25	234	0.4	0.1 M KOH	35
$Ni_{0.9}Fe_{0.1}O_X$	1.2	1065	0.3	1.0 M KOH	36
RuO_2/defective CeO_2	360	~52	0.4	0.1 M KOH	37
γ-CoOOH nanosheets	150	66.6	0.3	1.0 M KOH	38
γ-CoOOH bulk	150	3.4	0.3	1.0 M KOH	38
$Ca_2Mn_2O_5$	255	30	0.4	0.1 M KOH	39
IrO_2	116	86	0.5	0.1 M KOH	This work
1 nm BSCF-Ni	1.4	9006	0.5	0.1 M KOH	This work
5 nm BSCF-Ni	8.4	1631	0.5	0.1 M KOH	This work
10 nm BSCF-Ni	16.8	1517	0.5	0.1 M KOH	This work
15 nm BSCF-Ni	23.6	655	0.5	0.1 M KOH	This work
20 nm BSCF-Ni	38.7	271	0.5	0.1 M KOH	This work
20 nm BSCF-Ni foam	38.7	625	0.5	0.1 M KOH	This work

Note: Overpotential is defined relative to the thermodynamic potential for water splitting reaction of 1.23 V versus reversible hydrogen electrode (RHE).

The mass activity of 1 nm BSCF-Ni is 252 $mA\ mg^{-1}$ at an overpotential of 0.38 V, which is still more than 2 times that of the state-of-the-art IrO_2 nanoparticles (r-IrO_2 in Table S1, Ref 22).

To rule out the possible contribution of OER activity from the underlying Ni substrate (such as in the case of incomplete coverage of nanofilm on top of the substrate when pinholes or defects formed), we have subtracted the current density of the Ni substrate from the current density of the 1 nm BSCF-Ni sample on the original data (not on the iR-corrected data). At a low overpotential point of 0.5 V, for example, the normalized mass activity of the 1 nm BSCF-Ni nanofilm was 5078 $mA\ mg^{-1}$, which is still 178 times higher than that of the crystalline BSCF powder.

table S2. Comparison of the overpotentials to obtain 10 mA cm^{-2}_{film} for the ITO-based heterostructures and the Ni foil–based heterostructures.

ITO-based samples	Overpotential (V)	Ni foil-based samples	Overpotential (V) calibrated to single face	Overpotential (V) calibrated to double faces
1 nm	**0.54**	**1 nm**	**0.49**	**0.52**
2 nm	**0.50**	**5 nm**	**0.49**	**0.52**
5 nm	**0.54**	**10 nm**	**0.46**	**0.49**
10 nm	**0.52**	**15 nm**	**0.48**	**0.51**
15 nm	**0.56**	**20 nm**	**0.50**	**0.54**

The overpotential of the Ni foil-based heterostructures was substantially lower than those exhibited by the ITO-based samples at an identical mass loading (not including the 2 nm BSCF-ITO heterostructure). The intrinsic activity of the Ni foil-based heterostructures was still higher even after normalization by the two opposing geometric areas of the Ni foil.

table S3. Comparison of the performance of the water-splitting catalysts in a 1.0 M KOH solution.

Anode	Cathode	Loading (μg cm^{-2})	Onset potential (V)	Potential difference (V) @10 mA cm^{-2}	Reference
Co-P	Co-P	3710	1.56	n.a.	40
IrO_2	Pt/C	1000	1.47	n.a.	40
Ni/NiP	Ni/NiP	10580	1.50	1.61	41
Ni/IrO_2	Ni/Pt/C	11000	>1.50	>1.61	41
$NiCo_2O_4$	$Ni_{0.33}Co_{0.67}S_2$	300	1.60	n.a.	42
NiSe/NF	NiSe/NF	2800	n.a.	1.63	43
Pt/NF	Pt/NF	2800	n.a.	1.67	43
CP/CTs/Co-S	CP/CTs/Co-S	320	n.a.	1.74	44
RuO_2	Pt/C	320	n.a.	1.68	44
EG/$Co_{0.85}$Se/NiFe-LDH	EG/$Co_{0.85}$Se/NiFe-LDH	4000	n.a.	1.66	45
Ir/C	Pt/C	4000	n.a.	1.62	45
Ni_5P_4 Films/Ni	Ni_5P_4 Films/Ni	3500	n.a.	<1.70	46
Pt	Pt	n.a.	n.a.	>1.80	46
SNCF-NR	SNCF-NR	3000	~1.55	1.68	47
IrO_2	Pt/C	3000	~1.47	1.55	47
20 nm BSCF-Ni foam	10 nm Pt-Ni foam	38.7	1.50	1.62	This work
4*20 nm BSCF-Ni foam	4*10 nm Pt-Ni foam	154.8	1.44	1.57	This work

movie S1. Video of a water-splitting device.